Improved Oxygen Reduction Performance of Pt–Ni Nanoparticles by Adhesion on Nitrogen-Doped Graphene

ARTICLE *in* THE JOURNAL OF PHYSICAL CHEMISTRY C · JANUARY 2014

Impact Factor: 4.77 · DOI: 10.1021/jp4101619

3 AUTHORS:

Eduardo Gracia Espino
Umeå University
29 PUBLICATIONS **257** CITATIONS
SEE PROFILE

Xueen Jia
Umeå University
30 PUBLICATIONS **492** CITATIONS
SEE PROFILE

Thomas Wågberg
Umeå University
119 PUBLICATIONS **1,412** CITATIONS
SEE PROFILE

THE JOURNAL OF PHYSICAL CHEMISTRY C

Article

pubs.acs.org/JPCC

Improved Oxygen Reduction Performance of Pt−Ni Nanoparticles by Adhesion on Nitrogen-Doped Graphene

Eduardo Gracia-Espino,[†,‡] Xueen Jia,[‡] and Thomas Wågberg*[,‡]

[†]Department of Chemistry, Umeå University, 901 87 Umeå, Sweden

[‡]Department of Physics, Umeå University, 901 87 Umeå, Sweden

ABSTRACT: Graphene and its derivatives hold great potential as support for nanocatalyst in various energy applications, such as fuel cells, batteries, and capacitors. In this work, we used density functional theory to analyze substrate effect on the electrocatalytic activity of Pt−Ni bimetallic nanoparticles for oxygen reduction reaction (ORR). The dissociative mechanism is used to evaluate the ORR performance (energy barrier for O_2 dissociation, free energy of intermediates, d-band center, overpotential, and electrochemical activity) for a Pt−Ni core−shell-like nanoparticle ($PtNi_{CS}$) deposited on nondefective graphene (GS) or nitrogen-doped graphene (N-GS). The electronic and catalytic properties of $PtNi_{CS}$ on N-GS designate N-doped graphene as the best substrate to use for ORR, showing better interaction with the bimetallic cluster, improved charge transfer between constitutes, and a superior ORR performance when compared to $PtNi_{CS}$ on GS. The N-GS has a significant effect in reducing the energy barrier for O_2 dissociation and decrease the energetic stability of HO* intermediates, resulting in enhanced ORR activity compared with the $PtNi_{CS}$ on GS. In addition, the strong interaction between $PtNi_{CS}$ cluster and N-GS substrate may lead to an improved long-term stability of the catalytic particle during ORR cycles.

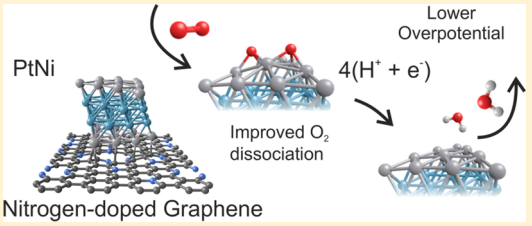

INTRODUCTION

Polymer electrolyte membrane fuel cells (PEMFC) represent a promising alternative for energy production with low environmental impact. Current commercial electrocatalysts implemented in PEMFCs are based on Pt-alloy metallic nanoparticles dispersed on various carbon supports. However, the existence of a substantial overpotential (η_{ORR}) for oxygen reduction reaction (ORR) in combination with catalyst dissolution limits the real-life applications. Recent studies have shown that Pt-bimetallic nanoparticles exhibit an improved ORR activity and stability relative to pure Pt.[1−8] The concept of bimetallic nanoparticles has therefore come into focus, especially regarding surface modification of the nanoparticle composition at the atomic scale.[1−3] In particular, core−shell structures, comprising a noble metal allocated at the surface and a low-cost, earth-abundant metal as core, have shown to exhibit excellent electrocatalytic properties. Stamenkovic et al.[4] and others attributed the outstanding catalytic ORR performance of a segregated Pt_3Ni (111) alloy,[4,5] with Pt atoms in the outermost surface layer and Ni atoms in the second atomic layer, with lattice distortion generated by the Ni core, modifying the electronic structure of Pt by shifting its d-band center.[1,4−6] Even more recently, the synthesis of polyhedral (octahedral, cuboctahedral, etc.) Pt−Ni nanoparticles with specific surface composition have shown an additionally improved oxygen reduction activity.[7,8]

Anchoring nanocatalyst on carbon substrates or other supports adds an additional parameter to the electrocatalyst system. A supports primary task is to hinder agglomeration of nanoparticles, keeping them firmly attached to offer a long-term stability, allowing a good fuel diffusion and finally to offer a high electron conductance between nanoparticle and the bulk electrode. Studies of hybrid systems, comprising metallic or semiconducting nanoparticles supported on diverse carbon substrates, exhibiting all the mentioned advantages have been reported in several key studies over the past years.[9−12] However, besides having these attributes, a good support might also alter the catalytic performance of the catalyst nanoparticles, and a proper interaction between nanoparticle and support might lead to changes in the electronic properties of both catalyst and support and thereby boost the overall catalytic performance. Such effects have shown to give strong synergistic effects for important catalytic reactions, such as ORR.[13,14] However, despite some experimental observations of enhanced catalytic performance originating from substrate effects, the theoretical understanding of such systems is limited.

In our work, we studied the influence of nitrogen-doped graphene (N-GS) substrate on the oxygen reduction performance of anchored platinum−nickel core−shell ($PtNi_{CS}$) nanoparticles by means of density functional theory (DFT) and compared with $PtNi_{CS}$ nanoparticles deposited on the corresponding undoped graphene substrate (GS). Both carbon supports have shown extraordinary performance as catalyst support for various applications.[12−15] For both systems we have analyzed the substrate effect on the electronic properties, charge transfer, oxygen dissociation, overpotential, ORR

Received: October 13, 2013
Revised: January 12, 2014
Published: January 13, 2014

   dx.doi.org/10.1021/jp4101619 | J. Phys. Chem. C 2014, 118, 2804−2811

activity, and the d-band center of the $PtNi_{CS}$ clusters. We show that the N-GS has a significant effect in reducing the energy barrier for O_2 dissociation and decreasing the energetic stability of HO* intermediates, resulting in enhanced ORR activity compared with the $PtNi_{CS}$ on GS. Furthermore, the strong interaction between $PtNi_{CS}$ cluster and N-GS substrate may lead to an improved long-term stability of the catalytic particle during ORR cycles. Our study is important for both a fundamental understanding of physical and chemical interactions at the nanoscale as well as for technological development of state-of-the art catalyst systems.

COMPUTATIONAL METHODS

Electronic Properties Calculation. Density functional theory (DFT) calculations were performed using the SIESTA code[16] within the local density approximation.[17] Electron exchange-correlation functionals are represented with the generalized gradient approximation (GGA) and the model of Perdew, Burke, and Ernzerhof (PBE)[18] for the nonlocal corrections. The wave functions for the valence electrons are represented by a linear combination of pseudoatomic numerical orbitals[19] using double-ζ basis for carbon and nitrogen and double-ζ plus one polarized orbital for hydrogen, oxygen, palladium, and nickel. The real-space grid used for charge and potential integration is equivalent to a plane wave cutoff energy of 350 Ry. Periodic boundary conditions are used and the intergraphene distance is kept to a minimum of 40 Å to avoid interactions. The integration of the Brillouin zone was carried out using $1 \times 8 \times 8$ Monkhorst–Pack grid[20] and Fermi–Dirac smearing with a width of 0.1 eV is employed to aid convergence. The density of states (DOS) is obtained using a $1 \times 16 \times 16$ Monkhorst–Pack grid. Because of the 2D system periodicity, both the total energy and atomic forces are corrected by a self-consistent dipole correction. All systems are fully relaxed until the maximum force is <0.04 eV/Å.

Material Design. Octahedral clusters are built from the face-centered cubic (FCC) motif. First bulk coordinates of Pt and Ni are obtained, and then a supercell is cut, forming an octahedral cluster containing 44 atoms. Four different clusters are produced: (1) Pt_{44}, (2) Ni_{44}, (3) $PtNi_{alloy}$, and (4) $PtNi_{CS}$. The octahedral nanoparticles, with FCC arrangement, reveals the (111) crystal plane in their eight faces. The $PtNi_{alloy}$ nanoparticle is produced by replacing one Pt atom with Ni from the FCC unit cell generating a 1.2:1 Pt:Ni alloy. On the other hand, the $PtNi_{CS}$ is obtained by replacing the two inner Pt layers from the octahedral Pt_{44} nanoparticle by Ni atoms, resulting in a 1:1.2 Pt:Ni cluster (see Figure 3 for more details). We use two different surfaces to analyze the effect of the substrate: (1) nondefective graphene supercell (GS) containing 240 carbon atoms (~2.6 × 2.5 nm); (2) nitrogen-doped graphene (N-GS) created by introducing five pyridine-like islands and 11 substitutional nitrogens on GS, resulting in ~11 at. % of nitrogen. In both cases the $PtNi_{CS}$ clusters were initially collocated in the central region at 2.5 Å above the graphene and then geometrically optimized. The adsorption energy (E^X_{ads}) is defined as $E^X_{ads} = E_{total} - E_{subs} - E_X$, where X is the O_2 molecule or $PtNi_{CS}$ cluster. E_{total} is the energy of the entire system (substrate + adsorbate), and the E_{subs} (E_X) refers to the energy of the isolated substrate (adsorbate).

Free Energy Diagrams. First, the ORR is initiated by the adsorption of one O_2 molecule on a hollow (fcc) site of the metallic nanoparticle. After the O_2 dissociation, four hydrogen atoms (one at the time) are introduced to proceed with the ORR. The free energies of intermediates in the electrochemical reactions were calculated based on the computational hydrogen electrode (CHE) model suggested by Nørskov et al.[21] The CHE model defines that at standard conditions (pH = 0 in the electrolyte and 1 bar of H_2 in the gas phase at 298.15 K) the chemical potential of a proton–electron pair ($H^+ + e^-$) in solution is equal to half of the chemical potential of a gas-phase H_2 molecule. The Gibbs free energy change (ΔG_0) of intermediates is calculated by $\Delta G_0 = \Delta E + \Delta ZPE - T\Delta S$, where ΔE is the energy change obtained from DFT calculations, ΔZPE is the change in zero-point energies, T is temperature (298.15 K), and ΔS is the change in entropy. Standard values of zero-point energies and entropies for the ORR intermediates are obtained from ref 21. The effect of a bias on states involving electron transfer results in a direct shift in the free energy of the electrons, and it can be included by correcting the Gibbs free energy (ΔG_U) by $-eU$, where U is the applied bias and e is the number of electrons transferred. Therefore, by computing the adsorption energies of the intermediates in the ORR allows to calculate the overall free energy pathway as a function of the applied bias; thus, the total change in free energy is given by $\Delta G = \Delta G_0 + \Delta G_U$.

Charge Analysis. The Bader charge analysis[22,23] was used to determine the transferred electronic charge among components using the optimized geometries and 350 Ry as energy cutoff for the real-space grid. The charge density difference $\delta n(\mathbf{r})$ of $PtNi_{CS}$-N-GS is obtained by subtracting the charge densities of N-GS ($n(\mathbf{r})_{slab}$) and $PtNi_{CS}$ ($n(\mathbf{r})_{PtNics}$) from the total charge density of $PtNi_{CS}$-N-GS ($n(\mathbf{r})_{total}$), $\delta n(\mathbf{r}) = n(\mathbf{r})_{total} - n(\mathbf{r})_{slab} - n(\mathbf{r})_{PtNics}$. The charge densities of N-GS and $PtNi_{CS}$ are computed from the isolated components maintaining the geometry in the optimized structure of the $PtNi_{CS}$-N-GS system.

The activation energy barrier (E_a) and the corresponding transition states (TS) for O_2 dissociation on $PtNi_{CS}$ cluster were computed using the nudged elastic band (NEB) method[24] as implemented in the Quantum Espresso (QE) code.[25] After the initial and final configurations of a reaction path are known, the intermediate configurations are determined by a linear interpolation followed by energy minimization across the minimum-energy path. The electronic structure was solved using ultrasoft pseudopotentials[26] and the GGA-PBE approximation. The kinetic energy cutoff for wave functions was set to 30 and 350 Ry for the charge density. A Marzari–Vanderbilt[27] smearing of 0.02 Ry is used to aid convergence.

RESULTS AND DISCUSSION

Oxygen Reduction Reaction on Octahedral Nanoparticles. We start our analysis of the catalytic properties for ORR of four different octahedral nanoparticles: (1) Pt_{44}, (2) Ni_{44}, (3) $PtNi_{alloy}$, and (4) $PtNi_{CS}$. We studied the dissociative mechanism for oxygen reduction by means of DFT using the computational hydrogen electrode (CHE) model proposed by Nørskov et al.[21] The reaction scheme for the dissociative mechanism, a four-electron pathway, is depicted in Figure 1 and involves the dissociation of a previously adsorbed O_2 molecule (step 2) into atomically adsorbed oxygen (step 3) followed by four proton–electron pair ($H^+ + e^-$) transfer, producing two water molecules without generating H_2O_2 as intermediate. Figure 1 shows the optimized geometries of the intermediates generated during the ORR, and the corresponding elementary reactions are indicated in eqs 1–6, where an asterisk denotes adsorbed species.

dx.doi.org/10.1021/jp4101619 | J. Phys. Chem. C 2014, 118, 2804–2811

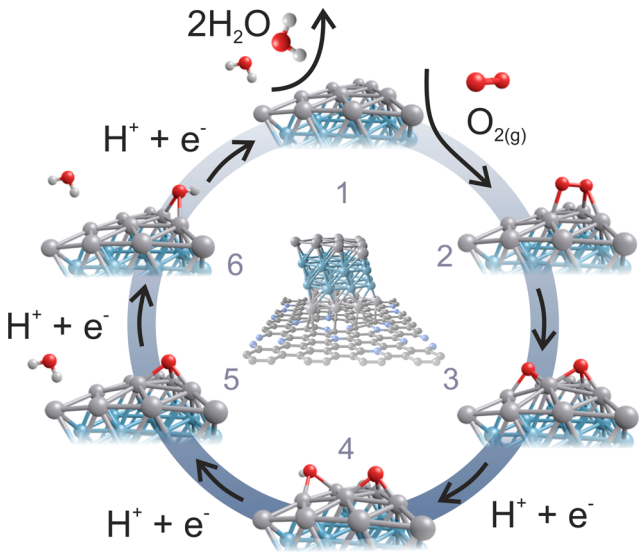

Figure 1. Reaction scheme of the dissociative mechanism for the oxygen reduction reaction (ORR). The scheme shows the optimized geometries for the ORR performed on $PtNi_{CS}$ nanoparticle anchored on nitrogen-doped graphene ($PtNi_{CS}$-N-GS). The dissociative mechanism involves the dissociation of a previously adsorbed O_2 (step 2) into atomically adsorbed oxygens (step 3) followed by four proton−electron pairs ($H^+ + e^-$) transfer producing two water molecules without generating H_2O_2 as intermediate.

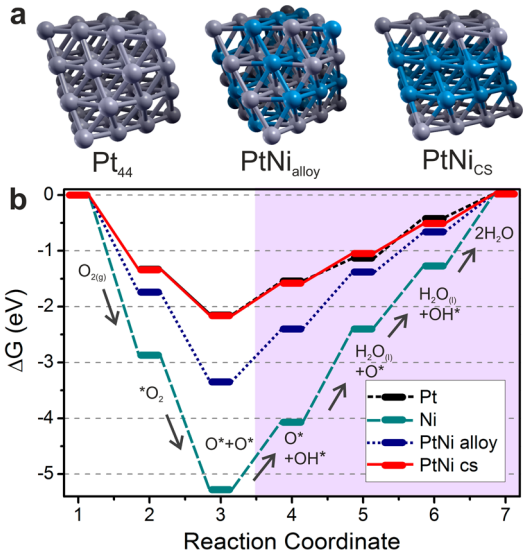

Figure 2. (a) Octahedral Pt_{44}, $PtNi_{alloy}$, and $PtNi_{CS}$ clusters. (b) Change in Gibbs free energy (ΔG) during ORR on four different catalytic nanoparticles at the equilibrium potential (U_0) of 1.23 V. Pt_{44} (short dashed line), Ni_{44} (long dashed line), $PtNi_{alloy}$ (dotted line), and $PtNi_{CS}$ (solid line). The reaction coordinates indicate the ORR reaction steps illustrated in Figure 1. In all cases, the first two ($H^+ + e^-$) transfers are the most endergonic steps.

$$O_{2(g)} \rightarrow O_2^* \quad (1)$$

$$O_2^* \rightarrow O^* + O^* \quad (2)$$

$$O^* + O^* + (H^+ + e^-) \rightarrow O^* + HO^* \quad (3)$$

$$O^* + HO^* + (H^+ + e^-) \rightarrow O^* + H_2O_{(l)} \quad (4)$$

$$O^* + H_2O_{(l)} + (H^+ + e^-) \rightarrow HO^* + H_2O_{(l)} \quad (5)$$

$$HO^* + H_2O_{(l)} + (H^+ + e^-) \rightarrow 2H_2O_{(l)} \quad (6)$$

The optimized geometries of Pt_{44} (Ni_{44} exhibit similar structure), $PtNi_{alloy}$, and $PtNi_{CS}$ are depicted in Figure 2a. The change in Gibbs free energy (ΔG) during the chemical reactions, shown in eqs 1−6, at equilibrium potential (U_0) for ORR equal to 1.23 V are plotted in Figure 2b. We observe that Ni_{44} cluster exhibit the largest oxygen adsorption energy ($E^{O2}{}_{ads}$) and after dissociation, the atomically adsorbed oxygen is highly stabilized (ΔG_2 = 2.4 eV), contrary to the Pt_{44} cluster which exhibits the lowest $E^{O2}{}_{ads}$ and the 2O* intermediate has a ΔG_2 = 0.8 eV. For the $PtNi_{alloy}$ cluster, we observed an intermediate behavior with a larger $E^{O2}{}_{ads}$ than Pt_{44} cluster, and the 2O* intermediate is highly stabilized (ΔG_2 = 1.6 eV) as in the case of Ni_{44}.

This is a consequence of the $PtNi_{alloy}$ atomic arrangement, since the Ni atoms located at the surface strongly interact with oxygen, especially $*O_2$ and 2O*, inhibiting further reactions and decreasing the ORR activity. However, this is not the case for all PtNi mixtures; when the Pt−Ni distribution is modified to a core−shell-like structure $PtNi_{CS}$, the adsorption of molecular and atomic oxygen (eqs 1 and 2) behaves similarly as pure Pt_{44} but with an $E^{O2}{}_{ads}$ that is 0.1 eV larger than Pt_{44} and a 2O* intermediate which is destabilized by 0.1 eV. Both changes represent an improvement on the ORR performance, since higher $E^{O2}{}_{ads}$ will help to easily overcome the energy barrier for oxygen dissociation, and the destabilized 2O* intermediate decreases the overall uphill energy that may result in lowering the oxygen reduction overpotential (η_{ORR}). The subsequent four proton−electron ($H^+ + e^-$) transfers (steps 4−7), shown as shadow area in Figure 2b, are uphill in free energy, indicating that the reactions in eqs 3−6 are thermodynamically hindered at U_0. As proposed by Nørskov et al.,[21] the largest of these steps is directly related with the η_{ORR}; therefore, the free energy distribution along these four steps is important. We find that the total uphill energy for $PtNi_{CS}$, along the four ($H^+ + e^-$) steps, is reduced and distributed differently compared to pure Pt_{44}. As a result, the $PtNi_{CS}$ has a η_{ORR} equal to 0.58 eV compared to Pt_{44} where the η_{ORR} = 0.71 eV, in both cases the limiting step is related with HO* formation. On the other hand, the η_{ORR} of $PtNi_{alloy}$ is 1.02 and 1.67 eV for Ni_{44}; in both cases, the large η_{ORR} is a consequence of Ni atoms at the surface, which exhibit a strong interaction with O-intermediates and therefore inhibits further chemical reactions. Here the η_{ORR} for Pt_{44} is larger than the obtained for periodic $Pt_{(111)}$ surfaces due higher adsorption energy of O_2 and O-intermediates generated by size effects.[28−30] The observed reduction of η_{ORR} for Pt−Ni core−shell structures has been previously reported and is attributed to the lattice strain introduced by the Ni-core generating a shift in the d-band center of the Pt shell.[1,6]

$PtNi_{CS}$ Chemisorbed on Nitrogen-Doped Graphene. In order to analyze the effect of the substrate on the ORR performance, we placed the $PtNi_{CS}$ cluster on nondefective graphene (GS) and nitrogen-doped graphene (N-GS) surfaces. The $PtNi_{CS}$ deposited on nondefective graphene ($PtNi_{CS}$-GS) exhibit an adsorption energy ($E^{PtNi}{}_{ads}$) equal to −0.77 eV. On the other hand, the $PtNi_{CS}$ deposited on N-GS ($PtNi_{CS}$-N-GS) exhibit a larger $E^{PtNi}{}_{ads}$ = −0.86 eV. The larger $E^{PtNi}{}_{ads}$ for $PtNi_{CS}$-N-GS is related to an improved chemical reactivity of N-doped nanocarbons, rationalizing the formation of several Pt−C bonds, where mainly the C atoms around the N_3-islands

dx.doi.org/10.1021/jp4101619 | J. Phys. Chem. C 2014, 118, 2804−2811

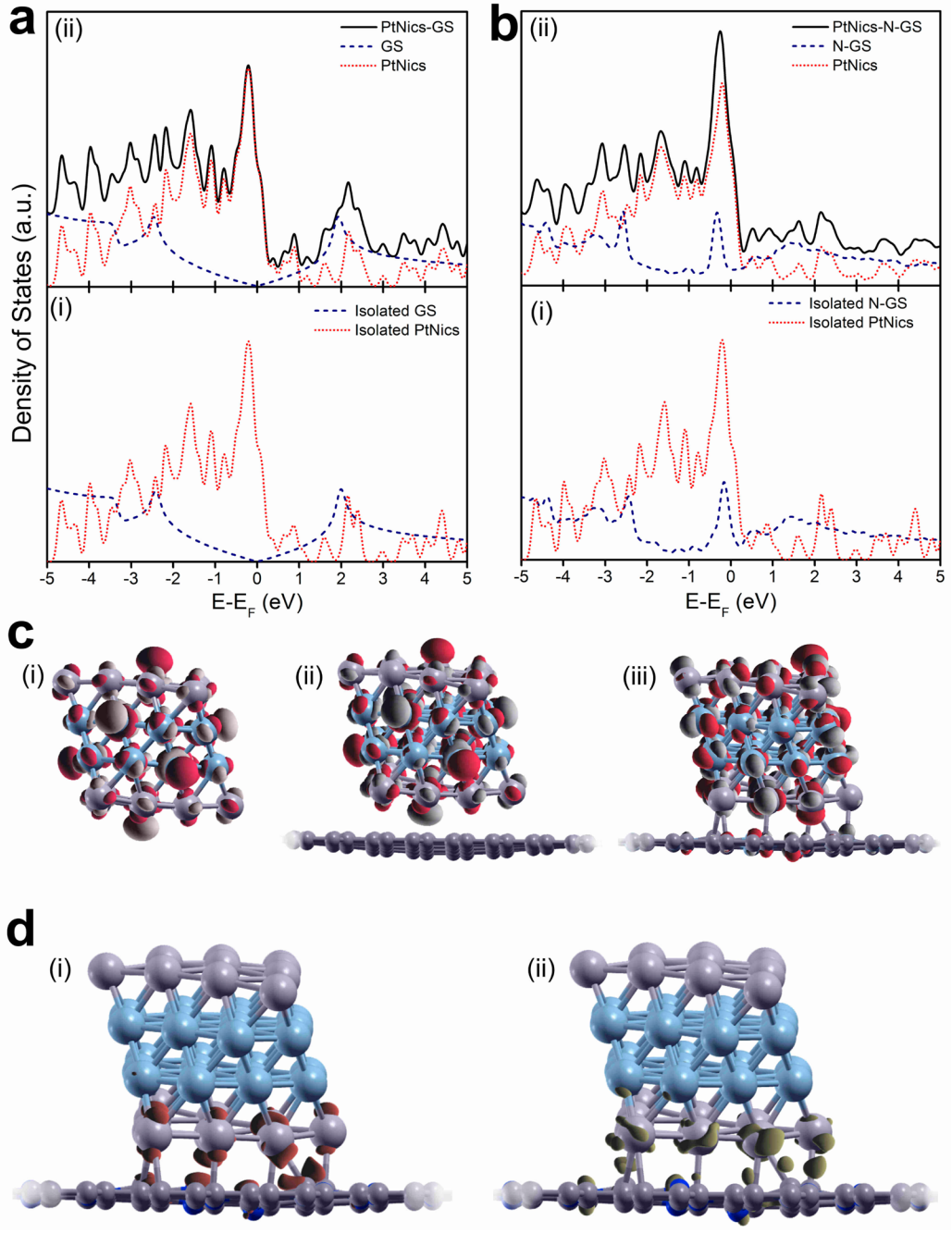

Figure 3. Electronic density of states (DOS) of (a) $PtNi_{CS}$-GS and (b) $PtNi_{CS}$-N-GS systems. (c) Isosurface wave functions of the HOMO of $PtNi_{CS}$, $PtNi_{CS}$-GS, and $PtNi_{CS}$-N-GS; the isosurfaces value is ±0.03 e Å^{-3}. In (c-ii), the $PtNi_{CS}$ does not exhibit any chemical bond to the GS substrate, and the cluster is located ∼3.5 Å above the substrate. On the other hand, in (c-iii), the $PtNi_{CS}$-N-GS composite exhibits one Pt−N and seven Pt−C chemical bonds. (d) Difference charge density, $\delta n(\mathbf{r})$, of the $PtNi_{CS}$-N-GS hybrid system. (d-i) indicates the areas with a depletion of charge density after the $PtNi_{CS}$ interaction with N-GS substrate, while (d-ii) illustrates areas where an increment is observed; the isosurfaces value is ±0.004 e^-.

participate in the chemical bonding to the $PtNi_{CS}$ cluster due to a strong electron localization on pyridine-like nitrogen.[15,31,32]

The resulting electronic properties can be understood by analyzing the electronic density of states (DOS) for both composite systems and isolated components. The results for $PtNi_{CS}$-GS are shown in Figure 3a; panel (i) depicts the DOS of the isolated $PtNi_{CS}$ and the isolated GS (before adsorption), while panel (ii) shows the DOS for $PtNi_{CS}$-GS composite (adsorbed state) together with the projected DOS (PDOS) of its components. From Figure 3c-ii it can be observed that the graphene substrate of the $PtNi_{CS}$-GS system is slightly deformed after cluster adsorption, but no chemical bonds are found between the cluster and the substrate, where the $PtNi_{CS}$ is located at ∼3.5 Å above the GS. However, the $PtNi_{CS}$-GS DOS (Figure 3a-ii) is essentially a superposition of the electronic states arising from isolated systems (see panel (i)). The PDOS indicates that the states near the Fermi level (FL) arise from the localized electronic states of the metal nanocluster, while the graphene substrate remains in semimetallic state after the deposition of the $PtNi_{CS}$ cluster,

dx.doi.org/10.1021/jp4101619 | J. Phys. Chem. C 2014, 118, 2804−2811

suggesting that the electronic properties of pristine graphene are not significantly altered, in agreement with previous reports for nondefective SWCNTs and graphene.[33,34] In contrast, the $PtNi_{CS}$-N-GS system exhibits new chemical bonds, and the local geometry at the binding site is modified for both components which explains the change in the PDOS for the adsorbed state (Figure 3b-ii) in comparison with the isolated components (Figure 3b-i). As observed in Figure 3c-iii, the $PtNi_{CS}$ deposited on the doped substrate exhibits one Pt−N and seven Pt−C bonds with an average bond length of 2.33 and 2.36 Å, respectively. Noteworthy is also that, in this case, the graphene does not lose its planar structure.

In order to clarify the change in electronic properties, the isosurface wave functions corresponding to the highest occupied molecular orbital (HOMO) for the $PtNi_{CS}$, $PtNi_{CS}$-GS, and $PtNi_{CS}$-N-GS systems are plotted in Figure 3c. For the isolated cluster, the HOMO wave function is symmetric along the particle with larger localization on the central atom of each surface. After adsorption of $PtNi_{CS}$ on GS, the HOMO wave function remains almost identical to the isolated cluster, and no states are observed on GS. As a consequence, the electronic properties of the adsorbed metallic cluster are similar to the isolated $PtNi_{CS}$. A different situation occurs when N-GS is used as substrate. The carbon atoms surrounding the pyridine-like island strongly interact with the metallic cluster, and the resulting HOMO wave function is very different from the isolated cluster, with a distinct loss in symmetry. This suggests that the properties of the clusters are now different along the surfaces, contrary to the isolated case where the Pt or Ni surfaces are equivalent. There is also a clear localization of electrons on the N-GS near the binding sites and on N atoms distributed along the substrate.

Our studies are complemented by analyzing the electronic charge transfer between the cluster and graphene substrates. Using the Bader analysis,[23,24] we find, in the $PtNi_{CS}$-GS system, a charge flow from GS to $PtNi_{CS}$ cluster of 0.07 electrons (e^-), resulting in a p-type doping for the GS substrate. The directionality of charge transfer relies on the work function of both the metallic cluster (Φ_M) and the graphene substrate (Φ_G). Considering that bulk Pt has a Φ_{Pt} = 6.13 eV[35] and bulk Ni has a Φ_{Ni} = 5.35 eV,[36] the resulting Φ_{PtNi} can easily promote the charge transfer from graphene to the metallic cluster, consistent with our Bader analysis. Instead, when the N-GS is used as substrate, the magnitude and direction of charge transfer are different, and we find that 0.13 e^- is transferred from the catalytic particle to the doped substrate. Considering that nitrogen doping on graphene substantially decrease the work function,[37,38] one would intuitively expect a charge transfer from N-GS to $PtNi_{CS}$, in contrast to what we find. The explanation for that apparent controversy is the generation of the new chemical bonds in the $PtNi_{CS}$-N-GS system, which localizes electronic charge between the metal cluster and the substrate. The electrons participating in these new bonds originate mainly from the $PtNi_{CS}$ particle, resulting in a depletion of electronic charge in the metallic cluster. To visualize this, we calculated the difference in electron charge density, $\delta n(\mathbf{r})$, so that the charge transfer regions in $PtNi_{CS}$-N-GS system could be observed. Figure 3d-i shows the regions with a depletion of charge density, whereas the Figure 3d-ii indicates regions with a gain of electrons. As we see, the density charge redistribution occurs around the new chemical bonds, between the cluster and the substrate, supporting the formation of chemical bonds.

Oxygen Reduction on $PtNi_{CS}$-N-GS Composite. Using the CHE model and following the chemical reactions in eqs 1−6, we have determined the electrocatalytic properties of $PtNi_{CS}$-GS and $PtNi_{CS}$-N-GS composites for ORR. The change in free energy is shown in Figure 4. We observe two important

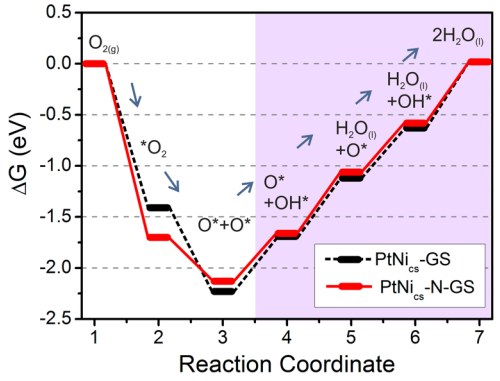

Figure 4. Change in Gibbs free energy (ΔG) during ORR performed on $PtNi_{CS}$ anchored on two different substrates: nondefective graphene ($PtNi_{CS}$-GS, dashed line) and nitrogen-doped graphene ($PtNi_{CS}$-N-GS, solid line). The adsorption of O_2 on $PtNi_{CS}$-N-GS (step 2) is stabilized by 0.29 eV compared with $PtNi_{CS}$-GS; nevertheless, the atomically adsorbed O is destabilized by 0.1 eV (step 3). The following four proton−electron ($H^+ + e^-$) transfers are similar in both materials. However, the $PtNi_{CS}$-N-GS system exhibits the lowest η_{ORR}.

improvements for the ORR on the $PtNi_{CS}$-N-GS compared to the $PtNi_{CS}$-GS. The first improvement is related to the adsorption of molecular oxygen on $PtNi_{CS}$-N-GS (step 2) which is stabilized by 0.29 eV, when compared to the $PtNi_{CS}$-GS system. The second is related to the atomically adsorbed 2O*, which is destabilized by 0.1 eV (step 3), similarly as the $PtNi_{CS}$ and Pt_{44} case seen in Figure 2. The four proton−electron ($H^+ + e^-$) transfer steps are similar in both materials. However, the lower free energy of 2O* intermediate on $PtNi_{CS}$-N-GS, and the homogeneous distribution of the ($H^+ + e^-$) steps, in total results in lower overpotential for the ORR (η_{ORR} = 0.61 eV for $PtNi_{CS}$-N-GS compared to η_{ORR} = 0.65 eV for $PtNi_{CS}$-GS). Now, both η_{ORR} are slightly larger than the isolated case (η_{ORR} = 0.58 eV), which is related to the higher energetic stability of HO* intermediates on both composite materials. Here it is however worth to mention that isolated nanoparticles are very difficult to realize experimentally, since these would readily agglomerate into larger particles. Therefore, a proper support is essential to anchor the nanoparticles.

In total, we observe a more efficient oxygen reduction process for the $PtNi_{CS}$-N-GS system in comparison with the $PtNi_{CS}$-GS, and we ask ourselves from where exactly these improvements originate? According to the dissociative mechanism and the CHE model, the oxygen dissociation is the sole step that has an energy barrier. It is therefore important to identify its corresponding activation energy (E_a). As observed from Figure 4, the $E^{O2}{}_{ads}$ in $PtNi_{CS}$-N-GS is larger compared with the isolated $PtNi_{CS}$ and the $PtNi_{CS}$-GS, and this will have a direct effect on E_a due the Brønsted−Evans−Polanyi (BEP) behavior.[39,40] The E_a for $PtNi_{CS}$ cluster, $PtNi_{CS}$-GS, and $PtNi_{CS}$-N-GS systems shown in Figure 5 is illustrated by the reaction energy and the transition state (TS) during O_2 dissociation (chemical reaction in eq 3). Specifically, the E_a and the TS were determined using the nudge elastic band

dx.doi.org/10.1021/jp4101619 | J. Phys. Chem. C 2014, 118, 2804−2811

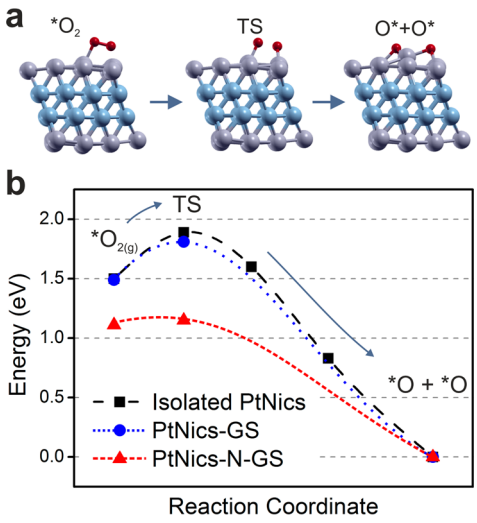

Figure 5. (a) Initial, transition state (TS), and final geometries for O_2 dissociation reaction on isolated $PtNi_{CS}$. (b) Activation energy (E_a) and the TS for O_2 dissociation on the $PtNi_{CS}$ nanoparticle in three different situations. (1) Isolated $PtNi_{CS}$ cluster (squares), (2) $PtNi_{CS}$-GS (circles), and (3) $PtNi_{CS}$-N-GS (triangles). The E_a for the $PtNi_{CS}$-GS (0.32 eV) system is similar to the isolated case (0.35 eV) because the low interaction between the nanoparticle and graphene. However, when N-GS is used as substrate, the E_a is reduced to 0.04 eV. $PtNi_{CS}$ data are obtained by the NEB method. The E_a for composites are obtained according to eq 7. The lines are guides to the eyes.

(NEB) method[24] for the $PtNi_{CS}$ system, and because of the excellent agreement with the linear BEP relationship proposed by Michaelides et al.,[41] the corresponding E_a for $PtNi_{CS}$-GS and $PtNi_{CS}$-N-GS systems can be derived using the following linear relationship for diatomic activations[41] (eq 7):

$$E_a\ (\text{eV}) = (0.97 \pm 0.05)\Delta E_{ads}^{O2} + 1.69 \pm 0.15 \qquad (7)$$

The E_a obtained from the NEB calculation is equal to 0.35 eV for the isolated $PtNi_{CS}$, which is very close to 0.39 eV obtained using eq 7. Now, by using eq 7, we observe that the O_2 dissociation on $PtNi_{CS}$-GS exhibits an E_a = 0.32 eV, similarly to the isolated case. This is in line with expectations because of the low interaction between the metallic cluster and GS substrate. However, when the $PtNi_{CS}$ cluster is chemisorbed on N-GS, the E_a for O_2 dissociation is considerably reduced, exhibiting a value of E_a = 0.04 eV. Similar results have been observed on Pt deposited on defective graphene.[29] Table 1 shows a comparison for diverse parameters related to the different systems, and the superiority of the N-doped systems is obvious. Although we note that the composite might not show an improved ORR performance, since the rate-limiting step is still the $(H^+ + e^-)$ transfer, it is clear that the improved interaction between cluster and substrate will have a positive effect on the long-term stability of the catalytic particle due the restricted atomic movements at the binding site. Additionally, the lower E_a for O_2 dissociation in the $PtNi_{CS}$-N-GS system will promote the dissociation mechanism for ORR where a $4e^-$ pathway is followed, and avoid the generation of H_2O_2 as subproduct (a $2e^-$ reduction).

Table 1. Adsorption Energy, Activation Barrier, and ORR Overpotential

system	$E(PtNi_{CS,ads})$ (eV)	$E(O_{2,ads})$ (eV)	$E_a{}^a$ (eV)	η_{ORR} (eV)
Ni_{44}		−2.87	−1.10	1.67
Pt_{44}		−1.33	0.40	0.71
$PtNi_{alloy}$		−1.74	0.01	1.02
$PtNi_{CS}$		−1.34	0.39	0.58
$PtNi_{CS}$-GS	−0.77	−1.41	0.32	0.65
$PtNi_{CS}$-N-GS	−0.86	−1.70	0.04	0.61
bulk $Pt_{(111)}$		−1.21	0.52	0.45[21]

[a]Data obtained using the $E^{O2}{}_{ads}$ and eq 7.

Charge Transfer Analysis during ORR. The charge transfer can substantially affect the electronic properties of any of the components in the systems, and analyzing the charge transfer can give us some insight about the effect of N-doped graphene as substrate. Using the Bader analysis, we illustrate the charge transfer events during ORR for the isolated $PtNi_{CS}$, $PtNi_{CS}$-GS, and $PtNi_{CS}$-N-GS systems in Figure 6. In all systems, the $PtNi_{CS}$ catalyst exhibits a depletion of electronic charge which is transferred to the ORR intermediates. As we previously described, before the ORR, the catalytic particle has a slightly negative charge ($0.07\ e^-$) in the $PtNi_{CS}$-GS system, a positive charge ($-0.13\ e^-$) in $PtNi_{CS}$-N-GS, and a neutral ($0.0\ e^-$) for the isolated $PtNi_{CS}$. The results in Figure 6 indicate that the charge transferred to ORR intermediates is independent of the presence and type of substrate. Similarly, the excess (depletion) of charge that N-doped (nondefective) graphene substrate has is basically constant during the reactions steps, being independent of any chemical reaction performed on the surface of the $PtNi_{CS}$ nanoparticle. As observed in Figure 6, the $PtNi_{CS}$ adsorbed on GS exhibits the lowest charge depletion due the previous addition of $0.07\ e^-$ from the substrate. This addition of electrons stabilizes the catalytic particle during the ORR, especially during for the process of adsorbing atomic oxygen (eq 2). As a consequence, we observed that the free energy of the $PtNi_{CS}$-GS at step 3, in Figure 4, is increased (stabilizing the system) by 0.1 eV compared to $PtNi_{CS}$-N-GS, resulting in larger change of free energy during $(H^+ + e^-)$ transfer and consequently larger η_{ORR}. In contrast, the $PtNi_{CS}$-N-GS composite exhibits a larger charge depletion which destabilizes the system, especially in steps 2 and 3, and as a result, it shows a reduction in free energy change during the $(H^+ + e^-)$ transfer and thereby an improved η_{ORR}.

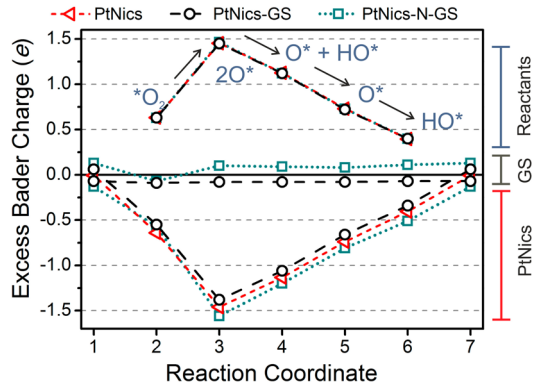

Figure 6. (a) Change in excess of Bader charge during the ORR for three different systems: (1) isolated $PtNi_{CS}$ (triangles), (2) $PtNi_{CS}$-GS (circles), and (3) $PtNi_{CS}$-N-GS (squares). In all systems, the $PtNi_{CS}$ particle exhibits a depletion of electronic charge which is transferred to the ORR intermediates. The $PtNi_{CS}$ particle on the N-GS system shows an extra loss of e^- ($-0.013\ e^-$) due to the charge localization on the N-GS vicinity, contrary to the $PtNi_{CS}$-GS, where the GS substrate transfers $0.07\ e^-$ to the catalytic particle.

dx.doi.org/10.1021/jp4101619 | J. Phys. Chem. C 2014, 118, 2804−2811

Finally, to make the comparison between systems easier, we calculated the activity volcano plot for ORR relative to Pt_{44} as a function of HO* free energy. According to Nørskov et al.,[42,43] the universal activity volcano plot for (111) facets is given by[42,43]

$$kT \ln\left(\frac{j_X}{j_{Pt44}}\right) = \Delta E_{OH,X} - \Delta E_{OH,Pt44} \quad (8)$$

$$kT \ln\left(\frac{j_X}{j_{Pt44}}\right) = 0.26 - 0.97(\Delta E_{OH,X} - \Delta E_{OH,Pt44}) \quad (9)$$

where k, T, and j are the Boltzmann constant, the temperature (298.15 K), and the electrical current density; eqs 8 and 9 describe the left and right side of the volcano plot, respectively. Here, to avoid size effects, we have used the Pt_{44} cluster as a reference material instead of the periodic $Pt_{(111)}$ surface. The volcano plot is shown in Figure 7a. All $PtNi_{CS}$ systems (isolated clusters and composites) exhibit slightly lower HO* free energy than Pt_{44}, resulting in higher ORR activity, which is related to the η_{ORR}. The two materials at the top of the volcano plot are the isolated $PtNi_{CS}$ and the $PtNi_{CS}$-N-GS composite. Both materials have similar ORR activity, which is slightly larger than the $PtNi_{CS}$-GS due to a higher HO* adsorption energy. The improved ORR performance can be also explained by the weaker interaction of oxygenated species with the cluster surface, due the shifting in the Pt d-band center.[4−6] In this case, the O* adsorption energy (ΔE^{O}_{ads}) as a function of the relative d-band center ($\varepsilon_d - \varepsilon_d^{Pt44}$), with respect to Pt_{44} cluster, is shown in Figure 7b. We found a clear linear relationship between ΔE^{O}_{ads} and the d-band center, where a lower $\varepsilon_d - \varepsilon_d^{Pt44}$ is observed for $PtNi_{CS}$ systems, which is in agreement with previous publications.[4−6] Here, the hybrid system with the doped substrate, $PtNi_{CS}$-N-GS, exhibit a lower d-band center than $PtNi_{CS}$ on the nondoped substrate. As a result, the $PtNi_{CS}$-N-GS exhibits weaker interaction with oxygenated species, resulting in lower η_{ORR}, which is consistent with our previous findings.

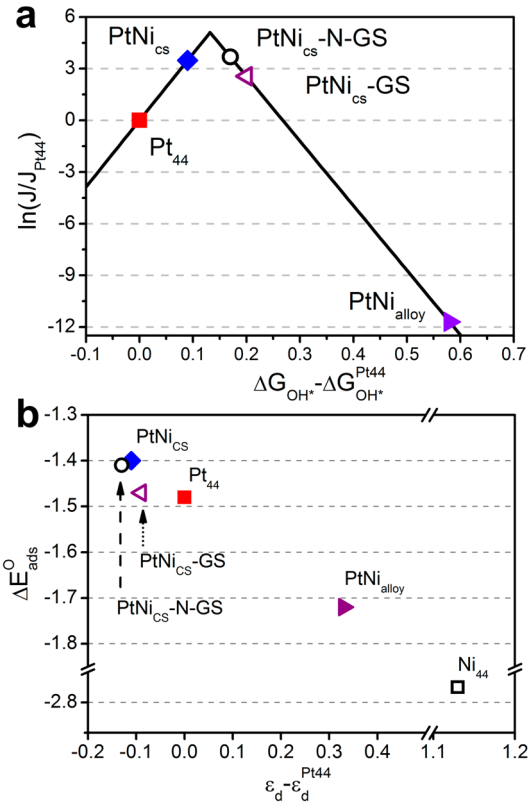

Figure 7. (a) Activity volcano plot for ORR as a function of HO* free energy. The isolated $PtNi_{CS}$ nanoparticle (diamond) exhibits the highest ORR activity when compared with the Pt_{44}, which is used as reference (square). For the $PtNi_{CS}$-N-GS (circle) the HO* adsorption energy decreases (with respect to Pt_{44}), resulting in a similar ORR activity as isolated $PtNi_{CS}$. Similarly, the $PtNi_{CS}$-GS system (empty triangle) exhibits an even lower HO* adsorption energy which decreases the ORR activity further. Besides Ni_{44} (not shown), the $PtNi_{alloy}$ (full triangle) exhibits the lowest ORR activity; the solid line is obtained using eqs 8 and 9. (b) Oxygen adsorption energy as a function of the relative d-band center ($\varepsilon_d - \varepsilon_d^{Pt44}$) with respect to Pt_{44} cluster.

CONCLUSIONS

We have reported a detailed and theoretical study of the electrocatalytic properties of hybrid systems made of N-doped graphene and Pt−Ni nanoparticles. We investigated the origin of the synergistic effect for ORR observed experimentally on diverse hybrid systems. We conclude that N-doped graphene strongly modify the energy barrier of O_2 dissociation, which will have significant impact on the oxygen reduction mechanism. We show that nitrogen-doped graphene substrate significantly decrease the O_2 dissociation barrier by promoting the dissociation mechanism. As a consequence, nitrogen-doped graphene will promote a $4e^-$ catalytic process for the supported Pt−Ni nanocatalyst. Overall, our results show major advantages as catalyst support for nitrogen-doped graphene compared to ordinary graphene, by offering better stabilization of the catalyst particles, improved electron transfer, enhanced long-term stability, and lower ORR overpotential.

AUTHOR INFORMATION

Corresponding Author

*E-mail: thomas.wagberg@physics.umu.se (T.W.).

Notes

The authors declare no competing financial interest.

ACKNOWLEDGMENTS

This work was supported by the Artificial Leaf Project Umeå (K&A Wallenberg foundation) and by the Swedish Research Council (grant 2010-3973). The theoretical calculations were performed on resources provided by the Swedish National Infrastructure for Computing (SNIC) at the High Performance Computing Center North (HPC2N). E.G.E. acknowledges support from CONACYT-Mexico grants (203575).

REFERENCES

(1) Xin, H.; Holewinski, A.; Linic, S. Predictive Structure-Reactivity Models for Rapid Screening of Pt-Based Multimetallic Electrocatalysts for the Oxygen Reduction Reaction. *ACS Catal.* **2012**, *2*, 12−16.

(2) Greeley, J.; Norskov, J. K. Combinatorial Density Functional Theory-based Screening of Surface Alloys for the Oxygen Reduction Reaction. *J. Phys. Chem. C* **2009**, *113*, 4932−4939.

(3) Ma, Y.; Balbuena, P. B. Surface Properties and Dissolution Trends of Pt3M Alloys in the Presence of Adsorbates. *J. Phys. Chem. C* **2008**, *112*, 14520−14528.

(4) Stamenkovic, V. R.; Fowler, B.; Mun, B. S.; Wang, G.; Ross, P. N.; Lucas, C. A.; Markovic, N. M. Improved Oxygen Reduction

Activity on Pt3Ni(111) via Increased Surface Site Availability. *Science* **2007**, *315*, 493−497.
(5) Stamenkovic, V.; Mun, B. S.; Mayrhofer, K. J. J.; Ross, P. N.; Markovic, N. M.; Rossmeisl, J.; Greeley, J.; Nørskov, J. K. Changing the Activity of Electrocatalysts for Oxygen Reduction by Tuning the Surface Electronic Structure. *Angew. Chem., Int. Ed.* **2006**, *45*, 2897−2901.
(6) Nørskov, J. K.; Abild-Pedersen, F.; Studt, F.; Bligaard, T. Density Functional Theory in Surface Chemistry and Catalysis. *Proc. Natl. Acad. Sci. U. S. A.* **2011**, *108*, 937−943.
(7) Cui, C.; Gan, L.; Li, H.-H.; Yu, S.-H.; Heggen, M.; Strasser, P. Octahedral PtNi Nanoparticle Catalysts: Exceptional Oxygen Reduction Activity by Tuning the Alloy Particle Surface Composition. *Nano Lett.* **2012**, *12*, 5885−5889.
(8) Zhang, J.; Yang, H.; Fang, J.; Zou, S. Synthesis and Oxygen Reduction Activity of Shape-Controlled Pt3Ni Nanopolyhedra. *Nano Lett.* **2010**, *10*, 638−644.
(9) Huang, X.; Qi, X.; Boey, F.; Zhang, H. Graphene-based Composites. *Chem. Soc. Rev.* **2012**, *41*, 666−686.
(10) Gracia-Espino, E.; Lopez-Urias, F.; Terrones, H.; Terrones, M. Novel Nanocarbons for Adsorption. In *Novel Carbon Adsorbents*; Tascon, J. M. D., Eds.; Elsevier: Oxford, 2012; pp 3−35.
(11) Hu, G.; Nitze, F.; Sharifi, T.; Barzegar, H. R.; Wågberg, T. Self-assembled Palladium Nanocrystals on Helical Carbon Nanofibers as Enhanced Electrocatalysts for Electro-oxidation of Small Molecules. *J. Mater. Chem.* **2012**, *22*, 8541−8548.
(12) Liang, Y.; Li, Y.; Wang, H.; Zhou, J.; Wang, J.; Regier, T.; Dai, H. Co_3O_4 Nanocrystals on Graphene as a Synergistic Catalyst for Oxygen Reduction Reaction. *Nat. Mater.* **2011**, *10*, 780−786.
(13) Zhang, L.; Niu, J.; Dai, L.; Xia, Z. Effect of Microstructure of Nitrogen-Doped Graphene on Oxygen Reduction Activity in Fuel Cells. *Langmuir* **2012**, *28*, 7542−7550.
(14) Sharifi, T.; Hu, G.; Jia, X.; Wågberg, T. Formation of Active Sites for Oxygen Reduction Reactions by Transformation of Nitrogen Functionalities in Nitrogen-Doped Carbon Nanotubes. *ACS Nano* **2012**, *6*, 8904−8912.
(15) Sharifi, T.; Gracia-Espino, E.; Barzegar, H. R.; Jia, X.; Nitze, F.; Hu, G.; Nordblad, P.; Tai, C.-W.; Wågberg, T. Formation of Nitrogen-Doped Graphene Nanoscrolls by Adsorption of Magnetic γ-Fe_2O_3 Nanoparticles. *Nat. Commun.* **2013**, 3319.
(16) Soler, J. M.; et al. The SIESTA Method for Ab Initio Order-N Materials Simulation. *J. Phys.: Condens. Matter* **2002**, *14*, 2745−2779.
(17) Kohn, W.; Sham, L. J. Self-Consistent Equations Including Exchange and Correlation Effects. *Phys. Rev.* **1965**, *140*, A1133.
(18) Perdew, J. P.; Burke, K.; Ernzerhof, M. Generalized Gradient Approximation Made Simple. *Phys. Rev. Lett.* **1996**, *77*, 3865−3868.
(19) Junquera, J.; Paz, Ó.; Sánchez-Portal, D.; Artacho, E. Numerical Atomic Orbitals for Linear-scaling Calculations. *Phys. Rev. B* **2001**, *64*, 235111.
(20) Monkhorst, H. J.; Pack, J. D. Special Points for Brillouin-Zone Integrations. *Phys. Rev. B* **1976**, *13*, 5188−5192.
(21) Nørskov, J. K.; Rossmeisl, J.; Logadottir, A.; Lindqvist, L.; Kitchin, J. R.; Bligaard, T.; Jonsson, H. Origin of the Overpotential for Oxygen Reduction at a Fuel-Cell Cathode. *J. Phys. Chem. B* **2004**, *108*, 17886−17892.
(22) Tang, W.; Sanville, E.; Henkelman, G. A Grid-based Bader Analysis Algorithm without Lattice Bias. *J. Phys.: Condens. Matter* **2009**, *21*, 084204.
(23) Sanville, E.; Kenny, S. D.; Smith, R.; Henkelman, G. An Improved Grid-Based Algorithm for Bader Charge Allocation. *J. Comput. Chem.* **2007**, *28*, 899−908.
(24) Henkelman, G.; Uberuaga, B. P.; Jonsson, H. J. A Climbing Image Nudged Elastic Band Method for Finding Saddle Points and Minimum Energy Paths. *Chem. Phys.* **2000**, *113*, 9901−9904.
(25) Giannozzi, P.; et al. Quantum Espresso: A Modular and Open-Source Software Project for Quantum Simulations of Materials. *J. Phys.:Condens. Matter* **2009**, *21*, 395502.
(26) Vanderbilt, D. Soft Self-Consistent Pseudopotentials in a Generalized Eigenvalue Formalism. *Phys. Rev. B* **1990**, *41*, 7892−7895.
(27) Marzari, N.; Vanderbilt, D.; De Vita, A.; Payne, M. C. Thermal Contraction and Disordering of the Al(1100) Surface. *Phys. Rev. Lett.* **1999**, *82*, 3296−3299.
(28) Stephens, I. E. L.; Bondarenko, A. S.; Grønbjerg, U.; Rossmeislc, J.; Chorkendorff, I. Understanding the Electrocatalysis of Oxygen Reduction on Platinum and Its Alloys. *Energy Environ. Sci.* **2012**, *5*, 6744−6762.
(29) Lim, D.-H.; Wilcox, J. Mechanism of the Oxygen Reduction Reaction on Defective Graphene-Supported Pt Nanoparticles from First-Principles. *J. Phys. Chem. C* **2012**, *116*, 3653−3660.
(30) Han, B. C.; Miranda, C. R.; Ceder, G. Effect of Particle Size and Surface Structure on Adsorption of O and OH on Platinum Nanoparticles: A First-Principles Study. *Phys. Rev. B* **2008**, *77*, 075410.
(31) Gracia-Espino, E.; López-Urías, F.; Terrones, H.; Terrones, M. Doping (10,0)-Semiconductor Nanotubes with Nitrogen and Vacancy Defects. *Mater. Express* **2011**, *1*, 127−135.
(32) Cruz-Silva, E.; Lopez-Urıas, F.; Munoz-Sandoval, E.; Sumpter, B. G.; Terrones, H.; Charlier, J.-C.; Meunier, V.; Terrones, M. Electronic Transport and Mechanical Properties of Phosphorus- and Phosphorus-Nitrogen-Doped Carbon Nanotubes. *ACS Nano* **2009**, *3*, 1913−1921.
(33) Subrahmanyam, K. S.; Manna, A. K.; Pati, S. K.; Rao, C. N. R. A Study of Graphene Decorated with Metal Nanoparticles. *Chem. Phys. Lett.* **2010**, *497*, 70−75.
(34) Ritz, B.; Heller, H.; Myalitsin, A.; Kornowski, A.; Martin-Martinez, F. J.; Melchor, S.; Dobado, J. A.; Juarez, B. H.; Weller, H.; Klinke, C. Reversible Attachment of Platinum Alloy Nanoparticles to Nonfunctionalized Carbon Nanotubes. *ACS Nano* **2010**, *4*, 2438−2444.
(35) Giovannetti, G.; Khomyakov, P. A.; Brocks, G.; Karpan, V. M.; Brink, J. V. D.; Kelly, P. J. Doping Graphene with Metal Contacts. *Phys. Rev. Lett.* **2008**, *101*, 026803.
(36) Baker, B. G.; Johnson, B. B.; Maire, G. L. C. Photoelectric Work Function Measurements on Nickel Crystals and Films. *Surf. Sci.* **1971**, *24*, 572−586.
(37) Kvashnin, D. G.; Sorokin, P. B.; Bruning, J. W.; Chernozatonskii, L. A. The Impact of Edges and Dopants on the Work Function of Graphene Nanostructures: The Way to High Electronic Emission From Pure Carbon Medium. *Appl. Phys. Lett.* **2013**, *102*, 183112.
(38) Luo, Z.; Lim, S.; Tian, Z.; Shang, J.; Lai, L.; MacDonald, B.; Fu, C.; Shen, Z.; Yu, T.; Lin, J. Pyridinic N Doped Graphene: Synthesis, Electronic Structure, and Electrocatalytic Property. *J. Mater. Chem.* **2011**, *21*, 8038−8044.
(39) Brønsted, N. Acid and Basic Catalysis. *Chem. Rev.* **1928**, *5*, 231−338.
(40) Evans, M. G.; Polanyi, N. P. Further Considerations on the Thermodynamics of Chemical Equilibria and Reaction Rates. *Trans. Faraday Soc.* **1936**, *32*, 1333−1360.
(41) Michaelides, A.; Liu, Z.-P.; Zhang, C. J.; Alavi, A.; King, D. A.; Hu, P. Identification of General Linear Relationships between Activation Energies and Enthalpy Changes for Dissociation Reactions at Surfaces. *J. Am. Chem. Soc.* **2003**, *125*, 3704−3705.
(42) Viswanathan, V.; Anton, H.; Rossmeisl, J.; Nørskov, J. K. Universality in Oxygen Reduction Electrocatalysis on Metal Surfaces. *ACS Catal.* **2012**, *2*, 1654−1660.
(43) Greeley, J.; Stephens, I. E. L.; Bondarenko, A. S.; Johansson, T. P.; Hansen, H. A.; Jaramillo, T. F.; Rossmeisl, J.; Chorkendorff, I.; Nørskov, J. K. Alloys of Platinum and Early Transition Metals as Oxygen Reduction Electrocatalysts. *Nat. Chem.* **2009**, *1*, 552−556.